Journal of Mathematical Chemistry, Vol. 39, No. 2, February 2006 (© 2005)
DOI: 10.1007/s10910-005-9034-0

Computational modelling of biosensors with perforated and selective membranes

R. Baronas *

Faculty of Mathematics and Informatics, Vilnius University, Naugarduko 24, LT-03225 Vilnius, Lithuania
E-mail: romas.baronas@maf.vu.lt

J. Kulys

Department of Chemistry and Bioengineering, Vilnius Gediminas Technical University, Sauletekio al. 11, LT-10223 Vilnius, Lithuania

F. Ivanauskas

Faculty of Mathematics and Informatics, Vilnius University, Naugarduko 24, LT-03225 Vilnius, Lithuania
Institute of Mathematics and Informatics, Akademijos 4, LT-08663 Vilnius, Lithuania

Received 18 July 2005; revised 12 August 2005

This paper presents a two-dimensional-in-space mathematical model of amperometric biosensors with perforated and selective membranes. The model is based on the diffusion equations containing a non-linear term of the Michaelis–Menten enzymatic reaction. Using numerical simulation of the biosensors action, the influence of the geometry of the perforated membrane on the biosensor response was investigated. The numerical simulation was carried out using finite-difference technique. The calculations demonstrated non-linear and non-monotonous change of the biosensor steady-state current at various degree of the surface of the perforated membrane covering. The non-monotonous behaviour of the biosensor response was also observed when changing the thickness of the perforated membrane.

KEY WORDS: modelling, reaction-diffusion, simulation, biosensor

AMS subject classification: 35K57, 65M06, 76R50, 92C45

1. Introduction

Biosensors are analytical devices consisting mainly of a biological entity that recognises the target analyte and the transducer that translates the biorecognition event into an electrical signal [1–3]. The signal is proportional to the

*Corresponding author.

concentration of the analyte. The biosensors are classified according to the nature of the physical transducer [4]. The amperometric biosensors measure the faradic current that arises on a working indicator electrode by direct electrochemical oxidation or reduction of the products of the biochemical reaction [5]. In amperometric biosensors the potential of the electrode is held constant while the current is measured. The amperometric biosensors are known to be reliable, cheap and highly sensitive for environment, clinical and industrial purposes [6,7].

A practical biosensor contains a multilayer enzyme membrane [1,8]. The electrode acting as a transducer of the biosensor is covered by selective membrane, following a layer of immobilized enzyme and an outer membrane. The outer membrane can be prepared from a dialysis membrane or, in modern biosensors, from perforated nucleopore type membrane [9]. The selective membrane is used to increase biosensors selectivity [10–12].

To improve the productivity and efficiency of biosensors design, to optimize the biosensors configuration a model of the real biosensors should be build [13–16]. The modelling of biosensors with perforated membranes has been performed by Schulmeister and Pfeiffer [17]. The model did not take into account the geometry of the holes in the membranes, included the diffusion coefficients having limited physical sense, and as authors recognized "its quantitative value is limited" [17]. The task of our investigation was to build the model approaching the real amperometric biosensor and to prepare friendly usable surrounding for the program use. By changing input parameters the output results were numerically analyzed with special emphasis to the influence of enzyme and membranes parameters to the response of biosensors at transition and steady-state conditions.

2. Principal structure

We assume that the thickness of the selective membrane as well as of the perforated membrane of a biosensor is much less than its length and width. In the biosensor, the selective membrane is of the uniform thickness. The holes in the perforated membrane were modelled by right cylinders. The holes are of uniform diameter and spacing, forming a hexagonal pattern. Figure 1 presents the biosensor schematically. Due to the uniform distribution of the holes, the entire biosensor may be divided into equal hexagonal prisms with regular hexagonal bases. For simplicity, it is reasonable to consider a circle whose area equals to that of the hexagon and to regard one of the cylinders as a unit cell of the biosensor. Due to the symmetry of the unit cell, we may consider only a half of the transverse section of the unit cell. Very similar approach has been used in modelling of partially blocked electrodes [18–20] and of a biosensor system based on an array of enzyme microreactors [21].

Figure 2 shows the profile of the unit of the biosensor, represented schematically in figure 1. In figure 2, a_2 is the radius of the base of the unit cell, while a_1 is the radius of the holes, b_1 stands for the thickness of the selective membrane,

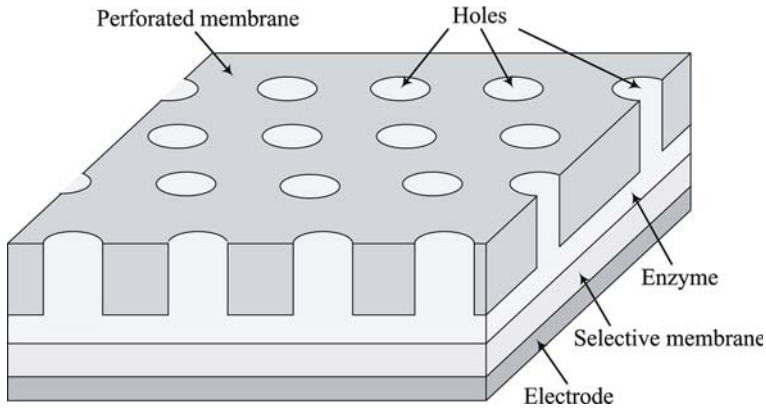

Figure 1. A principal structure of the biosensor. The figure is not to scale.

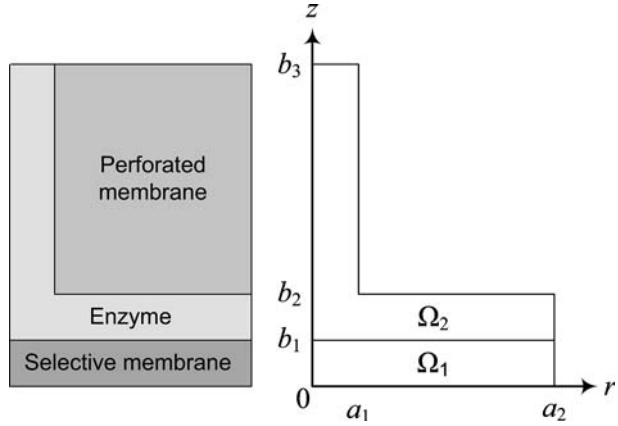

Figure 2. The profile of the unit cell at Y-plane. $z = 0$ represents the electrode surface, a_1 is the radius of holes, a_2 is the half distance between centres of adjacent holes. $d_1 = b_1$, $d_2 = b_2 - b_1$ and $d_3 = b_3 - b_2$ are the thickness of the selective membrane, the basic enzyme layer and the perforated membrane, respectively.

$d_3 = b_3 - b_2$ is the thickness the perforated membrane, $d_2 = b_2 - b_1$ is the thickness of the basic enzyme layer being between the selective and perforated membranes. We also assume that holes are filled with the enzyme.

3. Mathematical model

Let $\overline{\Omega}_1, \overline{\Omega}_2$ be closed regions, presented in figure 2, Γ_2 – the upper boundary of the region $\overline{\Omega}_2$,

$$\overline{\Omega}_1 = [0, a_2] \times [0, b_1], \tag{1}$$

$$\overline{\Omega}_2 = [0, a_2] \times [b_1, b_2] \cup [0, a_1] \times [b_2, b_3], \tag{2}$$

$$\Gamma_2 = [0, a_1] \times \{b_3\}. \tag{3}$$

Let Ω_i be the open region of the corresponding closed region $\overline{\Omega}_i$, $i = 1, 2$. In the region Ω_1 the mass (of the product only) transport by diffusion takes place, while in Ω_2 – the enzyme reaction and mass transport by diffusion takes place.

Governing equations ($0 < t \leqslant T$) are:

$$\frac{\partial P_1}{\partial t} = D_{1P}\,\Delta P_1, \quad (r, z) \in \Omega_1, \tag{4}$$

$$\frac{\partial S}{\partial t} = D_S \Delta S - \frac{V_{max} S}{K_M + S}, \qquad \frac{\partial P_2}{\partial t} = D_{2P}\,\Delta P_2 + \frac{V_{max} S}{K_M + S}, \quad (r, z) \in \Omega_2, \tag{5}$$

where Δ is the Laplace operator, $S = S(r,\ z,\ t)$ is the substrate concentration, $P_i = P_i(r,\ z,\ t)$ is concentration of the reaction product in the region $\overline{\Omega}_i$, D_S, D_{1P} and D_{2P} are the diffusion coefficients, V_{max} is the maximal enzymatic rate attainable with that amount of enzyme, when the enzyme is fully saturated with substrate, K_M is the Michaelis constant, and T is full time of the biosensor operation, $i = 1, 2$. The Laplace operator in cylindrical coordinates is described as follows [22]:

$$\Delta U = \frac{1}{r}\frac{\partial}{\partial r}\left(r\frac{\partial U}{\partial r}\right) + \frac{\partial^2 U}{\partial z^2}.$$

The initial ($t = 0$) conditions are as follows:

$$S(r,\ z, 0) = 0, \quad (r, z) \in \overline{\Omega}_2 \backslash \Gamma_2, \tag{6}$$

$$S(r, z,\ 0) = S_0, \quad (r, z) \in \Gamma_2, \tag{7}$$

$$P_k(r,\ z,\ 0) = 0, \quad (r, z) \in \overline{\Omega}_k, \quad k = 1, 2. \tag{8}$$

The following boundary conditions express the symmetry of the unit cell ($0 < t \leqslant T$)

$$\left.\frac{\partial P_1}{\partial r}\right|_{r=0} = \left.\frac{\partial P_1}{\partial r}\right|_{r=a_2} = 0, \quad z \in [0, b_1], \tag{9}$$

$$\left.\frac{\partial S}{\partial r}\right|_{r=0} = \left.\frac{\partial P_2}{\partial r}\right|_{r=0} = 0, \quad z \in [b_1, b_3], \tag{10}$$

$$\left.\frac{\partial S}{\partial r}\right|_{r=a_2} = \left.\frac{\partial P_2}{\partial r}\right|_{r=a_2} = 0, \quad z \in [b_1, b_2]. \tag{11}$$

The product is electro-active substance. The electrode potential is chosen to keep zero concentration of the product at the electrode surface. This is used in the following boundary condition ($0<t\leqslant T$):

$$P_1(r, 0, t) = 0, \quad r \in [0, a_2]. \tag{12}$$

On the boundary Γ_2 the concentrations of both species are maintained constant ($0<t\leqslant T$),

$$S(r, b_3, t) = S_0, \qquad P_2(r, b_3, t) = 0, \quad r \in [0, a_1]. \tag{13}$$

On the boundary of the perforated membrane we define non-leakage conditions ($0<t\leqslant T$),

$$\left.\frac{\partial S}{\partial r}\right|_{r=a_1} = \left.\frac{\partial P_2}{\partial r}\right|_{r=a_1} = 0, \quad z \in [b_2, b_3], \tag{14}$$

$$\left.\frac{\partial S}{\partial z}\right|_{z=b_2} = \left.\frac{\partial P_2}{\partial z}\right|_{z=b_2} = 0, \quad r \in [a_1, a_2]. \tag{15}$$

On the boundary between two adjusting regions we require the continuity of the concentration of the reaction product. On that boundary we also define non-leakage condition for the substrate ($0<t\leqslant T$),

$$\left.\frac{\partial S}{\partial z}\right|_{z=b_1} = 0, \quad D_{1\mathrm{P}} \left.\frac{\partial P_1}{\partial z}\right|_{z=b_1} = D_{2\mathrm{P}} \left.\frac{\partial P_2}{\partial z}\right|_{z=b_1},$$
$$P_1(r, b_1, t) = P_2(r, b_1, t), \quad r \in [0, a_2]. \tag{16}$$

The measured current is accepted as a response of biosensors in physical experiments. The current depends upon the flux of the reaction product at the electrode surface, i.e., at the border $z = 0$. Consequently, the density $I(t)$ (A/m^2) of the current at time t can be obtained explicitly from Faraday's and Fick's laws using the flux of the product concentration P_1 at the surface of the electrode,

$$I(t) = n_{\mathrm{e}} F D_{1\mathrm{P}} \frac{1}{\pi a_2^2} \int_0^{2\pi} \int_0^{a_2} \left.\frac{\partial P_1}{\partial z}\right|_{z=0} r \, \mathrm{d}r \mathrm{d}\varphi = n_{\mathrm{e}} F D_{1\mathrm{P}} \frac{2}{a_2^2} \int_0^{a_2} \left.\frac{\partial P_1}{\partial z}\right|_{z=0} r \, \mathrm{d}r, \tag{17}$$

where n_{e} is a number of electrons involved in a charge transfer at the electrode surface, F is Faraday constant, $F = 96485$ C/mol and φ is the third cylindrical coordinate.

We assume, that the system (4)–(16) approaches a steady-state as $t \to \infty$,

$$I_\infty = \lim_{t\to\infty} I(t). \tag{18}$$

4. Solution of the problem

Definite problems arise when solving analytically non-linear partial differential equations in domain of the complex geometry. Because of this the problem (4)–(18) was solved numerically using the finite difference technique [23,24]. To find a numerical solution of the problem in the domain $(\overline{\Omega}_1 \cup \overline{\Omega}_2) \times [0, T]$ we introduced a quasi-uniform grid $\overline{\omega}_{rh} \times \overline{\omega}_{zh} \times \overline{\omega}_\tau$,

$$
\begin{aligned}
\omega_{rh} &= \{r_i : r_i = r_{i-1} + h_{ri},\ i = 1, \dots, N_1, \dots, N_2 - 1,\ r_0 = 0,\ r_{N_1} = a_1,\ r_{N_2} = a_2\},\\
\omega_{zh} &= \{z_j : z_j = z_{j-1} + h_{zj},\ j = 1, \dots, M_1, \dots, M_2, \dots, M_3 - 1,\ z_0 = 0,\\
&\quad z_{M_1} = b_1,\ z_{M_2} = b_2,\ z_{M_3} = b_3\}\\
\omega_\tau &= \{t_n : t_n = t_{n-1} + \tau_{n-1}, \quad n = 1, \dots, K,\ t_0 = 0,\ t_K = T\},\\
\omega_{lrh} &= \{r : r \in \omega_{rh},\ a_{l-1} < r < a_l\},\\
\omega_{mzh} &= \{z : z \in \omega_{zh},\ b_{m-1} < z < b_m\},\\
\omega_{1h} &= \omega_{rh} \times \omega_{1zh},\\
\omega_{2h} &= (\omega_{rh} \times \omega_{2zh}) \cup (\omega_{1rh} \times \omega_{3zh}) \cup (\omega_{1rh} \times \{b_2\}) \cup (a_1, b_2),\\
\bar{\omega}_{lrh} &= \omega_{lrh} \cup \{a_{l-1}\} \cup \{a_l\},\\
\bar{\omega}_{mzh} &= \omega_{mzh} \cup \{b_{m-1}\} \cup \{b_m\},\\
\bar{\omega}_\tau &= \omega_\tau \cup \{0\},\\
\bar{\omega}_{1h} &= (\bar{\omega}_{rh} \times \bar{\omega}_{1zh}),\\
\bar{\omega}_{2h} &= (\bar{\omega}_{rh} \times \bar{\omega}_{2zh}) \cup (\bar{\omega}_{1rh} \times \bar{\omega}_{3rh}),\\
a_0 &= 0, \quad b_0 = 0,\ l = 1, 2,\ m = 1, 2, 3.
\end{aligned}
$$

We assume the following notations:

$$
\begin{aligned}
S_{ij}^n &= S(r_i, z_j, t_n), \quad (r_i, z_j, t_n) \in \bar{\omega}_{1h} \times \bar{\omega}_t,\\
P_{kij}^n &= P_k(r_i, z_j, t_n), \quad (r_i, z_j, t_n) \in \bar{\omega}_{kh} \times \bar{\omega}_t,\\
I_n &= I(t_n), \quad t_n \in \bar{\omega}_t, \quad k = 1, 2.
\end{aligned}
$$

Using alternating direction method a semi-implicit linear finite difference scheme has been built as a result of the difference approximation. The initial conditions (6)–(8) were approximated as follows

$$
\begin{aligned}
S_{ij}^0 &= 0, \quad (r, z) \in \bar{\omega}_{2h} \backslash \Gamma_2,\\
S_{ij}^0 &= S_0, \quad (r, z) \in \bar{\omega}_{2h} \cap \Gamma_2,\\
P_{kij}^0 &= 0, \quad (r, z) \in \bar{\omega}_{kh}, \quad k = 1, 2.
\end{aligned}
$$

To simplify the further notations we introduce the following difference operators:

$$\Lambda_r u_{ij}^n = \frac{1}{r_i h_{r,i+1/2}} \left(r_{i+1/2} \frac{u_{i+1,j}^n - u_{i,j}^n}{h_{r,i+1}} - r_{i-1/2} \frac{u_{ij}^n - u_{i-1,j}^n}{h_{ri}} \right),$$

$$\Lambda_z u_{ij}^n = \frac{1}{h_{z,j+1/2}} \left(\frac{u_{i,j+1}^n - u_{i,j}^n}{h_{z,j+1}} - \frac{u_{ij}^n - u_{i,j-1}^n}{h_{zj}} \right),$$

$$\Phi\, u_{ij}^n = \frac{V_{\max} u_{ij}^n}{K_{\mathrm{M}} + u_{ij}^n},$$

where $h_{r,i+1/2} = (h_{ri} + h_{r,i+1})/2$, $h_{z,j+1/2} = (h_{zj} + h_{z,j+1})/2$, $r_{i\pm1/2} = (r_i + r_{i\pm1})/2$.

Differential equations (4) and (5) were approximated by the following finite difference scheme:

$$\frac{P_{1ij}^{n+1/2} - P_{1ij}^n}{\tau_n/2} = D_{1\mathrm{P}} \left(\Lambda_r P_{1ij}^{n+1/2} + \Lambda_z P_{1ij}^n \right), \quad (r,z) \in \omega_{1h},$$

$$\frac{S_{ij}^{n+1/2} - S_{ij}^n}{\tau_n/2} = D_{\mathrm{S}} \left(\Lambda_r S_{ij}^{n+1/2} + \Lambda_z S_{ij}^n \right) - \Phi S_{ij}^n, \quad (r,z) \in \omega_{2h},$$

$$\frac{P_{2ij}^{n+1/2} - P_{2ij}^n}{\tau_n/2} = D_{2\mathrm{P}} \left(\Lambda_r P_{2ij}^{n+1/2} + \Lambda_z P_{2ij}^n \right) + \Phi S_{ij}^n, \quad (r,z) \in \omega_{2h},$$

$$\frac{P_{1ij}^{n+1} - P_{1ij}^{n+1/2}}{\tau_n/2} = D_{1\mathrm{P}} \left(\Lambda_r P_{1ij}^{n+1/2} + \Lambda_z P_{1ij}^{n+1} \right), \quad (r,z) \in \omega_{1h},$$

$$\frac{S_{ij}^{n+1} - S_{ij}^{n+1/2}}{\tau_n/2} = D_{\mathrm{S}} \left(\Lambda_r S_{ij}^{n+1/2} + \Lambda_z S_{ij}^{n+1} \right) - \Phi S_{ij}^{n+1/2}, \quad (r,z) \in \omega_{2h},$$

$$\frac{P_{2ij}^{n+1} - P_{2ij}^{n+1/2}}{\tau_n/2} = D_{2\mathrm{P}} \left(\Lambda_r P_{2ij}^{n+1/2} + \Lambda_z P_{2ij}^{n+1} \right) + \Phi S_{ij}^{n+1/2}, \quad (r,z) \in \omega_{2h},$$

$$n = 0, 1, \ldots, K-1,$$

where $t_{n+1/2} = t_n + 0.5\tau_n$.

The boundary and matching conditions (9)–(16) were approximated as follows:

$$P_{1i0}^n = 0, \quad i = 0, \ldots, N_2,$$

$$S_{iM_3}^n = S_0, \qquad P_{2iM_3}^n = 0, \quad i = 0, \ldots, N_1,$$

$$P_{10j}^n = P_{11j}^n, \qquad P_{1N_2j}^n = P_{1,N_2-1,j}^n, \quad j = 1, \ldots, M_1,$$

$$S_{0j}^n = S_{1j}^n, \qquad P_{20j}^n = P_{21j}^n, \quad j = M_1, \ldots, M_3,$$

$$S_{N_2j}^n = S_{N_2-1,j}^n, \qquad P_{2N_2j}^n = P_{2,N_2-1,j}^n, \quad j = M_1, \ldots, M_2,$$

$$S_{N_1j}^n = S_{N_1-1,j}^n, \qquad P_{2N_1j}^n = P_{2,N_1-1,j}^n, \quad j = M_2+1, \ldots, M_3,$$

$$S_{iM_2}^n = S_{i,M_2-1}^n, \qquad P_{2iM_2}^n = P_{2i,M_2-1}^n, \quad i = N_1+1, \ldots, N_2,$$

$$D_{1P}(P^n_{1iM_1} - P^n_{1iM_1-1})/h_{1M_1} = D_{2P}(P^n_{2iM_1+1} - P^n_{2iM_1})/h_{2M_1+1}, \quad i = 1, \ldots, N_2,$$
$$S^n_{iM_1} = S^n_{i,M_1+1}, \qquad P^n_{1iM_1} = P^n_{2iM_1}, \quad i = 1, \ldots, N_2.$$

The system of linear algebraic equations can be solved efficiently because of the tridiagonality of the matrix of the system.

Having numerical solution of the problem, the density of biosensor current at time $t = t_n$ is calculated by

$$I(t_n) = n_e F D_{1P} \frac{2}{a_2^2} \sum_{i=0}^{N_2-1} \frac{P^n_{1i1} - P^n_{1i0} + P^n_{1,i+1,1} - P^n_{1,i+1,0}}{2h_{z1}} r_{i+1/2} h_{r,i+1}, \quad n = 1, \ldots, K.$$

5. Digital simulation

In the digital simulation, the main problem is an overload of calculation due to the boundary conditions (12)–(13), and permissible conditions: $a_1 << a_2$ and $b_2 << b_3$. Due to the boundary conditions (12)–(13), to have an accurate and stable result it was required to use very small step size in z direction at the boundaries $z = 0$ and $z = b_3$. Because of the concavity of an angle at the point (a_1, b_2) is reasonable to use very small step size in both space directions: r and z at the boundaries $r = a_1$ and $z = b_3$. Due to the matching conditions (16), we used also small step size at the boundary $z = b_1$. We assume, that farther from all these peculiar boundaries, step size may increase in both space directions: r and z. Consequently, in the direction r, an exponentially increasing step size was used to both sides from a_1: to a_2 and to 0. In the direction z, an exponentially increasing step size was used form 0 to $b_1/2$, from b_1 down to $b_1/2$, from b_1 to $(b_1 + b_2)/2$, from b_2 down to $(b_1 + b_2)/2$, from b_2 to $(b_2 + b_3)/2$, and from b_3 down to $(b_2 + b_3)/2$.

Usually, alternating direction method does not restrict time increment. However, the step size in the direction of time is restricted due to the non-linear reaction term in (5), boundary conditions and the geometry of the domain. In order to achieve accurate and stable solution of the problem, at the beginning of the reaction-diffusion process we employed the restriction condition, which is usually used for fully explicit schemes [23,24],

$$\tau_0 < \frac{h^2_{r\min} h^2_{z\min}}{4D_{\max}(h^2_{r\min} + h^2_{z\min})},$$
$$D_{\max} = \max(D_S, D_{1P}, D_{2P}), \quad h_{r\min} = \min_{i=1,\ldots,N_2} h_{ri}, \quad h_{z\min} = \min_{j=1,\ldots,M_3} h_{zj}.$$

Since the biosensor action obeys the steady-state assumption when $t \to \infty$, it is reasonable to apply an increasing step size in the time direction. The final step size τ_{K-1} was in a few orders of magnitude higher than the first one τ_0.

The mathematical model as well as the numerical solution of the model was evaluated for different values of the maximal enzymatic rate $V_{\max}$, substrate concentration S_0 and different geometries of the perforated membrane. The following values of the parameters were constant in the numerical simulation of all the experiments:

$$\begin{aligned} &D_{1P} = 10^{-8}\,\mathrm{cm}^2/\mathrm{s}, \quad D_S = D_{2P} = 3 \times 10^{-6}\,\mathrm{cm}^2/\mathrm{s}, \\ &K_M = 10^{-7}\,\mathrm{mol}/\mathrm{cm}^3, \quad n_e = 2. \end{aligned} \tag{19}$$

The steady-state biosensor current I_∞ (the biosensor response) as well as the time moment of occurrence of the maximal current (response time) were assumed and analyzed as ones of the most important characteristics of biosensors.

In digital simulation, the biosensor response time was assumed as the time when the absolute current slope value falls below a given small value normalized with the current value. In other words, the time needed to achieve a given dimensionless decay rate ε is used,

$$T_R = \min_{i(t)>0} \left\{ t : \frac{1}{I(t)} \left| \frac{\mathrm{d}I(t)}{\mathrm{d}t} \right| < \varepsilon \right\}. \tag{20}$$

Consequently, the current at the response time T_R was assumed as the steady-state biosensor current I_∞. We employed $\varepsilon = 10^{-4}$. However, the response time $T = T_R$ as an approximate steady-state time is very sensitive to the decay rate ε, i.e., $T_R \to \infty$, when $\varepsilon \to 0$. Because of this, we employed a half of steady-state time to investigate the behaviour the response time [22]. The resultant relative output signal function $I^*(t)$ can be expressed as follows:

$$I^*(t) = \frac{I_R - I(t)}{I_R}, \quad I_R = I(T_R), \quad I_\infty = I_R, \tag{21}$$

where $I(t)$ is the output current density at time t as defined in (17), I_R is assumed as the steady-state current I_∞. Let us notice, that $0 \leqslant I^*(t) \leqslant 1$ at all $t \geqslant 0$, $I^*(0) = 1$ and $I^*(T_R) = 0$. Let $T_{0.5}$ be the time at which the reaction-diffusion process reaches the medium, called half-time of steady-state or, particularly, half of the time moment of occurrence of the maximal current, i.e., $I^*(T_{0.5}) = 0.5$.

The adequacy of the mathematical and numerical models was evaluated using known analytical solutions for amperometric biosensors with a single flat enzyme layer. At relatively low concentrations of the substrate, $S_0 << K_M$, the steady-state current can be calculated as follows [25]:

$$I_\infty = \lim_{t\to\infty} i(t) = n_e F D_S S_0 \frac{1}{d} \left(1 - \frac{1}{\cosh(\sigma)} \right), \tag{22}$$

$$\sigma^2 = \frac{V_{\max} d^2}{D_S K_M}, \tag{23}$$

where d is the thickness of the enzyme layer. The dimensionless factor σ^2 is known as the diffusion modulus (Damköhler number) [26]. In the case of flat one-layer biosensors the diffusion modulus σ^2 essentially compares the rate of enzyme reaction ($V_{\max}/K_M$) with the diffusion through the enzyme layer (d^2/D_S). The biosensor response is known to be under diffusion control when $\sigma^2 \gg 1$. If $\sigma^2 \ll 1$, then the enzyme kinetics predominates in the response.

In the case of very high substrate concentration, $S_0 \gg K_M$, the stationary current is expressed as follows [27]:

$$i_\infty = \frac{n_e F V_{\max} d}{2}. \tag{24}$$

The numerical solution of the model (4)–(17) was compared with the analytical ones (22) and (24), accepting $b_1 = 0$, $b_2 = b_3 = 12\mu$m and $a_1 = a_2$ at four values of $V_{\max}$: $10^{-9}, 10^{-8}, 10^{-7}, 10^{-6}$ mol/cm^3 s and two values of S_0 : $10^{-11}, 10^{-4}$ mol/cm^3. In all the cases, the relative difference between the numerical and analytical solutions was less than 1%.

6. Results and discussion

Using computer simulation we have investigated the dependence of the steady-state biosensor current as well as biosensor response time on the geometry of the membrane perforation. To investigate the effect of the relative radius of the holes, the radius a_1 of the holes was expressed through the radius a_2 of the unit cell, and the biosensor response was calculated at various values of a_1 and a_2,

$$a_1 = (1 - \alpha) a_2, \tag{25}$$

where α expresses the degree of covering of the surface of the perforated membrane. $(1 - \alpha)$ can be also called a relative radius of the holes. The case when $\alpha = 0$ $(a_1 = a_2)$ corresponds to a fully open (uncovered) enzyme layer, i.e., no perforated membrane appears on the enzyme layer. In that case $(a_1 = a_2)$, $b_3 - b_1$ is the thickness of the enzyme layer. The case of $\alpha = 1$ $(a_1 = 0)$ corresponds to another limiting case when the membrane has no holes, i.e., the biosensor has no contact with the substrate. Of course, no biosensor current rises in the case of $\alpha = 1$. If the area of the entire electrode surface equals A, then the area of all the halls equals $(1 - \alpha)^2 A$.

The steady-state biosensor current is very sensitive to changes of the maximal enzymatic rate $V_{\max}$ and substrate concentration S_0 [1, 2, 28]. Because of this, we investigate the influence of the geometry of the membrane perforation on

the biosensor response at different values of V_{max} and S_0. Changing values of these two parameters, the steady-state current I_∞ varies even in orders of magnitude. To evaluate the effect of the geometry of the membrane perforation on the biosensor response we normalize the biosensor current. Let $I_R(\alpha)$ be the steady state current of a biosensor, having the degree α of the surface covering. Thus $I_R(0)$ corresponds to the steady state current of a biosensor, having the radius of the holes a_1 coinciding to the radius a_2 of the unit cell, $a_1 = a_2$. We express the normalized steady-state biosensor current I_{RN} as the steady-state current of the biosensor, having perforated membrane upon the enzyme layer, divided by the steady-state current of the corresponding biosensor, having no perforated membrane upon the enzyme layer. Assuming $T_{0.5}(\alpha)$ as the half-time of the biosensor steady-state response at given relative radius $(1-\alpha)$ of the holes, we introduce the normalized half time $T_{0.5N}$,

$$I_{RN}(\alpha) = \frac{I_R(\alpha)}{I_R(0)}, \qquad T_{0.5N}(\alpha) = \frac{T_{0.5}(\alpha)}{T_{0.5}(0)}, \quad \alpha = 1 - \frac{a_1}{a_2}, \quad 0 \leqslant \alpha \leqslant 1. \tag{26}$$

Results of calculations at a_2=1μm, four values of V_{max}:1, 10, 100, 1000 nmol/cm^3 s and three values of S_0 : 1, 10, 100 nmol/cm^3 are depicted in figures 3 and 4. The radius a_1 of holes was changed from 0.05 to 1μm. Figure 3 presents the dependence of the biosensor current on the covering degree α. Figure 4 presents the dependence of the half time $T_{0.5N}$ of the steady state biosensor response on α.

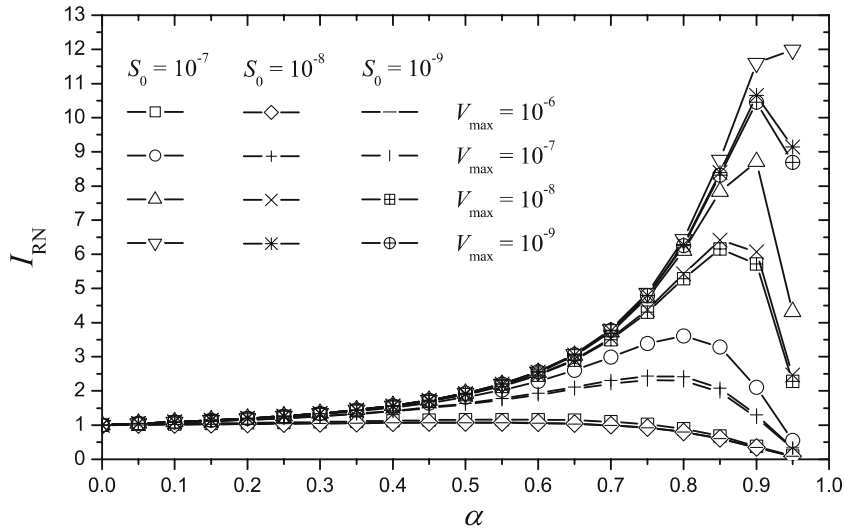

Figure 3. The normalized steady-state current I_{RN} versus the covering degree $\alpha = 1 - a_1/a_2$ at $a_2 = 1\mu$m, $d_1 = d_2 = 2\mu$m, $d_3 = 10\mu$m and different values of substrate concentration S_0 (mol/cm^3) as well as maximal enzymatic rate V_{max} (mol/cm^{3}s).

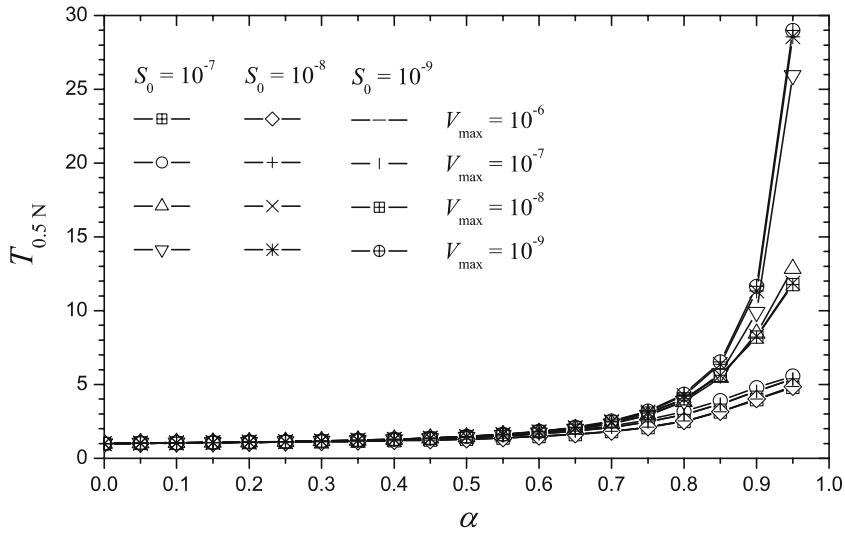

Figure 4. The normalized half-time $T_{0.5N}$ of the steady-state biosensor response versus the covering degree α. Values of all the parameters are the same as in figure 3.

One can see in figure 3, the steady-state current is a non-monotonous function of the dimensionless degree α of the covering of the perforated membrane surface. At low values of the ratio α, the steady state current increases with increase of α. Later the current starts to decrease. As it was mentioned above, in the case of fully closed membrane $I_{RN}(1)$ equals 0. The behaviour of biosensor response significantly depends on the maximal enzymatic activity V_{max}. At very high maximal enzymatic activity $V_{max}(10^{-6}\,\mathrm{mol/cm^3\,s})$ the steady state current I_R practically remains stagnant when the degree α increases from 0 to about 0.7. At $V_{max} = 10^{-6}\,\mathrm{mol/cm^3\,s}$, the maximum of the normalized current I_N equals approximately to 1.16 for $S_0 = 10^{-7}$ and 1.07 for $S_0 = 10^{-9}\,\mathrm{mol/cm^3}$. However, at low enzymatic rate $V_{max}(10^{-9}\,\mathrm{mol/cm^3\,s})$ the steady-state current I_R of the biosensor having perforated membrane onto the top of the enzyme layer, can generate the steady-state current which is more than 10 times higher than the current if the biosensor would be without the perforated membrane ($\alpha = 0$). For example, at $V_{max} = 10^{-9}\,\mathrm{mol/cm^3\,s}$, $S_0 = 10^{-7}\,\mathrm{mol/cm^3}$ and $\alpha = 0.95(a_1 = 0.05, a_2 = 1\mu\mathrm{m})$, $I_{RN} \approx 12\,(I_R(0.95) = 13.7, I_R(0) = 1.14\,\mathrm{nA/cm^2})$. This feature of biosensors with perforated and selective membranes can be applied in design of novel highly sensitive biosensors. Selecting the geometry of perforated membrane allows increasing the sensitivity of the biosensors.

Figure 4 shows the dependence of the half-time of the steady-state biosensor response on the ratio α. One can see in figure 4, the half-time $T_{0.5}$ increases monotonously with increasing α. This property is valid for all considered concentrations S_0 of the substrate and values of the maximal enzymatic rate V_{max}.

The gradient of change of $T_{0.5N}$ is especially high at low values of V_{max} and very small radiuses of holes, i.e., when α approaches to 1.

The parameter a_2 characterizes a frequency of the holes in the perforated membrane. A smaller value of a_2 corresponds to a higher density of the holes. To investigate the dependence of the biosensor response on the frequency of the holes we calculated the steady-state currents at constant radius $a_1=0.1\mu$m of holes changing a_2 from $a_1(\alpha=0)$ to $20a_1(\alpha=0.95)$. Results of calculations at different values of maximal enzymatic rate V_{max} and substrate concentration S_0 are depicted in figure 5. In this figure we see very similar shape of curves as in figure 3. Consequently, the absolute values of the radius a_1 of holes as well as the distance between adjacent holes have only weak influence on the biosensor response. The biosensor response depends mainly on the join factor α of the geometry of perforation. For example, at $V_{max}=10\,\text{nmol/cm}^3\,\text{s}$, $S_0=10\,\text{nmol/cm}^3$, $a_1=0.2$, $a_2=1\mu$m, the steady state current I_R equals to $11.1\,\text{nA/cm}^2$. In the case of two times greater radius of holes ($a_1=0.1$, $a_2=0.5\mu$m) and the same degree α, the current $I_R=11.5\,\text{nA/cm}^2$, i.e., I_R differs in several percents only. In both these cases, the covering degree α is the same, $\alpha=0.5$.

To investigate the dependence of the biosensor response on the thickness $d_3=(b_3-b_2)$ of the perforated membrane we calculated the biosensor response at constant radius $a_1=0.1\mu$m of holes, radius $a_2=1\mu$m ($\alpha=0.9$) of the cell, the thickness $d_1=b_1=2\mu$m of the selective membrane and the thickness $d_2=b_2-b_1=2\mu$m of the basic enzyme layer. The thickness d_3 of the perforated membrane varied from 1 to 20μm. In this case the current was normalized with respect to

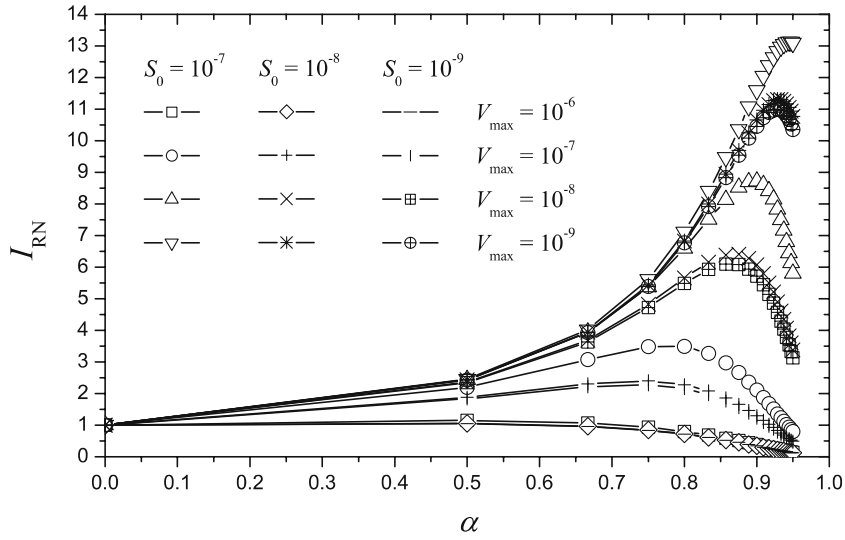

Figure 5. The normalized steady-state current I_{RN} versus the covering degree α at $a_1 = 0.1\mu$m changing a_2. Values of all other parameters are the same as in figure 3.

the minimal value d_{3m} of the thickness of the perforated membrane to be analyzed,

$$I_{\mathrm{p}}(d_3) = \frac{I_{\mathrm{R}}(d_3)}{I_{\mathrm{R}}(d_{3m})}, \quad d_3 \geqslant d_{3m} \geqslant 0, \quad d_3 = b_3 - b_2, \tag{27}$$

where $I_{\mathrm{p}}(d_3)$ is the normalized steady-state current, calculated at the thickness d_3 of the perforated membrane. Since in the numerical experiments d_3 varied from 1 to 20μm, then d_{3m}=1μm. Results of the calculations are depicted in figure 6, where one can see, that the effect of the thickness d_3 notably depends on the maximal enzymatic rate $V_{\max}$. At highest maximal enzymatic rate ($V_{\max}$ = 1μmol/cm^3 s) the steady-state current I_{R} decreases with increase of the thickness d_3, while at much lower value of $V_{\max}$=1 nmol/cm^{3}s, I_{R} is a monotonously increasing function of d_3. At moderate values of $V_{\max}$, I_{R} is a non-monotonous function of the thickness d_3 of the perforated membrane. The effect of the substrate concentration S_0 on the behaviour of the biosensor current is rather small.

Very similar behaviour of the biosensor response was observed when modelling one-layer biosensors acting in a non-stirred analyte [28]. Then the steady state biosensor current was found to be a monotonous decreasing function of the thickness of the external diffusion layer if the biosensor response is distinctly under diffusion control ($\sigma^2 >> 1$). In the cases when the enzyme kinetics controls the biosensor response ($\sigma^2 << 1$), the steady state current increases with increase of the thickness of the diffusion layer. Thus the steady state current

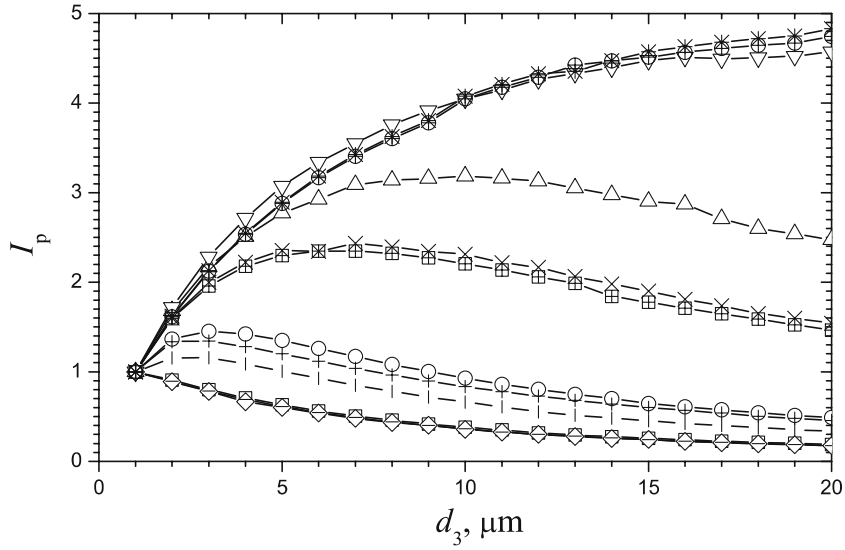

Figure 6. The normalized steady-state current I_3 versus the thickness $d_3 = (b_3 - b_2)$ of the perforated membrane at $a_1 = 0.1\mu$m, $a_2 = 10a_1$, $d_{3m} = 1\mu$m. Values of all other parameters and notation are the same as in figure 3.

varied up to several times. When $\sigma^2 \approx 1$, the variation of the steady state current is rather small.

On the other hand, assuming the perforated membrane as the periodic media, the homogenization process can be applied to the domain of the perforated membrane [29]. After this, the perforated membrane may be modelled as an external diffusion layer with the averaging diffusion coefficient [17]. So, the effect of the thickness of the perforated membrane on the biosensor response could probably be explained by the effect of the diffusion layer external to basic enzyme layer. In the case when the homogenization is applied, 1-D formulation of the mathematical model is enough. Unfortunately, the averaging diffusion coefficient cannot be calculated precisely and it has a limited physical sense. For comparison, in the case of 2-D formulation (4)–(17) of the model, no averaging diffusion coefficients are required and all the coefficients have clear physical sense.

To be sure, that the effect of the thickness of the perforated membrane on the biosensor response is really very similar to the effect of the thickness of the external diffusion layer, the calculations were repeated for several more values differing in an order of magnitude of the thickness d_2 of the basic enzyme layer. Results of the calculations showed that the behaviour of the biosensor response directly depends on thickness d_2 as well as on the maximal enzymatic rate $V_{\max}$. Thus we can conclude that the steady-state current I_R decreases with increase of the thickness d_3 of the perforated membrane when the biosensor response is distinctly under diffusion control, and I_R is a monotonous increasing function of d_3 when the enzyme kinetics controls the biosensor response.

The dependence of the biosensor response on the thickness $d_1 = b_1$ of the selective membrane was also investigated. The biosensor response was calculated at constant radius $a_1 = 0.1\mu$m of holes, radius $a_2 = 1\mu$m ($\alpha = 0.9$) of the cell, the thickness $d_3 = 10\mu$m of the selective membrane and the thickness $d_2 = 2\mu$m of the basic enzyme layer. In these calculations, the current was normalized with respect to the minimal value d_{1m} of the thickness of the selective membrane to be analyzed,

$$I_s(d_1) = \frac{I_R(d_1)}{I_R(d_{1m})}, \quad d_1 \geqslant d_{1m} \geqslant 0, \quad d_1 = b_1, \tag{28}$$

where $I_s(d_1)$ is the normalized steady-state current, calculated at the thickness d_1 of the selective membrane. The thickness d_1 of the perforated membrane varied from 0.5 to 10μm, $d_{1m} = 0.5\mu$m. Results of the calculations are depicted in figure 7. One can see in figure 7, that the effect of the thickness d_1 practically is independent from the maximal enzymatic rate $V_{\max}$ as well as from the substrate concentration S_0. I_R is a monotonously decreasing function of d_1 at all values of $V_{\max}$ and S_0 differing in orders of magnitude. The normalized currents were well

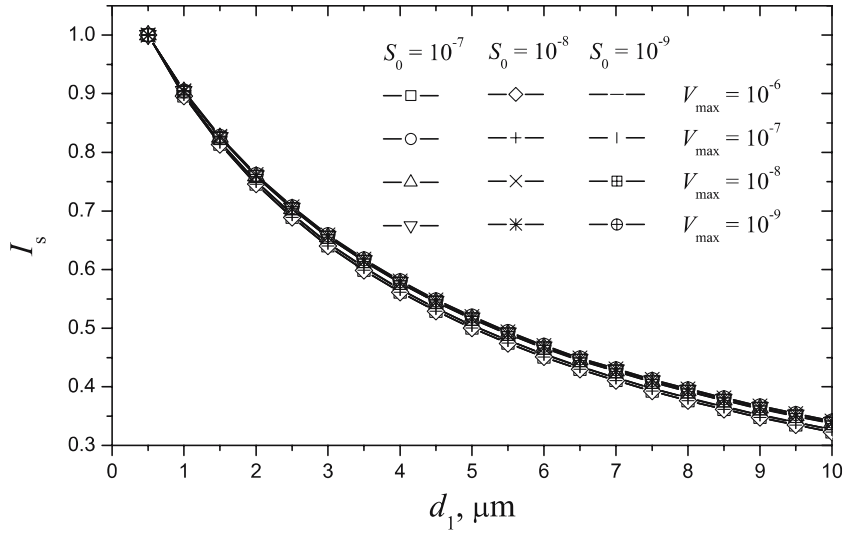

Figure 7. The normalized steady-state current I_s versus the thickness $d_1 = b_1$ of the selective membrane, $d_{1m} = 0.5\mu$m. Values of all other parameters and notation are the same as in figure 3.

fitted with the following exponential function:

$$I_s(d_1) = 0.27 + 0.81 \times \exp(-2500 d_1). \tag{29}$$

7. Conclusions

The mathematical model (4)–(17) of amperometric biosensors with perforated and selective membranes can be successfully used to investigate the kinetic peculiarities of the biosensor response (figure 1). The computer simulation of the biosensors can be used as a powerful tool in design of novel highly sensitive biosensors.

The steady-state current of the biosensor is a non-monotonous function of the dimensionless degree α of the covering of the surface of the perforated membrane (figures 3 and 5). The sensitivity of biosensors can be increased by selecting of the appropriate geometry of perforated membrane. The level of the possible increase of the sensitivity highly depends on the maximal enzymatic rate V_{max}. Significant gain in sensitivity can be achieved at low values of V_{max} only. The half-time $T_{0.5}$ of the steady-state biosensor response is a monotonous increasing function of α at wide range of substrate concentrations S_0 and maximal enzymatic rates V_{max} (figure 4).

The steady state current I_R decreases with increase of the thickness d_3 of the perforated membrane when the biosensor response is distinctly under

diffusion control, and I_R is a monotonous increasing function of d_3 when the enzyme kinetics controls the biosensor response (figure 6).

The steady state current I_R is an exponentially decreasing function of the thickness d_1 of the selective membrane at wide range of enzymatic activities V_{max} as well as substrate concentrations S_0 (figure 7). The thinner selective membrane is, the higher biosensor current is.

Acknowledgments

The work was partially supported by Lithuanian State Science and Studies Foundation, Project No. C-03048.

References

[1] A.P.F. Turner, I. Karube and G.S. Wilson, *Biosensors: Fundamentals and Applications* (Oxford University Press, Oxford, 1987).
[2] F. Scheller and F. Schubert, *Biosensors* (Elsevier Science, Amsterdam, 1992).
[3] G.G. Guilbault, *Analytical Uses of Immobilized Enzymes* (Marcel Dekker, New York, 1984).
[4] A. Chaubey and B.D. Malhotra, Biosens. Bioelectron. 17 (2002) 441.
[5] J. Rodriguez–Flores and E. Lorenzo, in: *Analytical Voltammetry*, eds. M.R. Smyth and J.G. Vos (Elsevier Science, Amsterdam, 1992) pp. 531–570.
[6] U. Wollenberger, F. Lisdat and F.W. Scheller, *Frontiers in Biosensorics 2: Practical Applications* (Birkhauser Verlag, Basel, 1997).
[7] K.R. Rogers, Biosens. Bioelectron. 10 (1995) 533.
[8] A.J. Baeumner, C. Jones, C.Y. Wong and A. Price, Anal. Bioanal. Chem. 378 (2004) 1587.
[9] R. Antiochia, I. Lavagnini and F. Magno, Anal. Lett. 37 (2004) 1657.
[10] D.S. Bindra, Y. Zhang, G.S. Wilson, R. Sternberg, D.R. Thévenot, D. Moatti and G. Reach, Anal. Chem. 63 (1991) 1692.
[11] D. Pfeiffer, F.W. Scheller, K. Setz and F. Schubert, Anal. Chim. Acta 281 (1993) 489.
[12] F.W. Scheller and D. Pfeiffer, Z. Chem. 18 (1978) 50.
[13] P.N. Bartlett and K.F.E. Pratt, Biosens. Bioelectron. 8 (1993) 451.
[14] D.G. Buerk, *Biosensors: Theory and Applications* (CRC Press, Lancaster, 1995).
[15] L.S. Ferreira, M.B. De Souza, J.O. Trierweiler, O. Broxtermann, R.O.M. Folly and B. Hitzmann, Comput. Chem. Eng. 27 (2003) 1165.
[16] T. Schulmeister, Selective Electrode Rev. 12 (1990) 260.
[17] T. Schulmeister and D. Pfeiffer, Biosens. Bioelectron. 8 (1993) 75.
[18] T. Gueshi, K. Tokuda and H. Matsuda, J. Electroanal. Chem. 89 (1978) 247.
[19] C. Deslous, C. Gabrielli, M. Keddam, A. Khalil, R. Rosset, B. Trobollet and M. Zidoune, Electrochim. Acta 42 (1997) 1219.
[20] R. Baronas, F. Ivanauskas and A. Survila, J. Math. Chem. 27 (2000) 267.
[21] R. Baronas, F. Ivanauskas, J. Kulys and M. Sapagovas, Nonlinear Anal. Model. Contr. 9 (2004) 203.
[22] J. Crank, *The Mathematics of Diffusion*, 2nd ed. (Clarendon Press, Oxford, 1975).
[23] D. Britz, *Digital Simulation in Electrochemistry*, 2nd ed. (Springer-Verlag, Berlin, 1988).
[24] A.A. Samarskii, *The Theory of Difference Schemes* (Marcel Dekker, New York–Basel, 2001).
[25] J. Kulys, Anal. Lett. 14 (1981) 377.
[26] R. Aris, *The Mathematical Theory of Diffusion and Reaction in Permeable Catalysts. The Theory of the Steady State* (Clarendon Press, Oxford, 1975).

[27] P.W. Carr and L.D. Bowers, *Immobilized Enzymes in Analytical and Clinical Chemistry: Fundamentals and Applications* (John Wiley, New York, 1980).
[28] R. Baronas, F. Ivanauskas and J. Kulys, Nonlinear Anal. Model. Contr. 8 (2003) 3.
[29] N.S. Bakhvalov and G.P. Panasenko, *Homogenization: Averaging Processes in Periodic Media* (Kluwer Academic Publishers, Dordrecht, 1989).